Pedalvatar: An IMU-Based Real-Time Body Motion Capture System Using Foot Rooted Kinematic Model

Yang Zheng Ka-Chun Chan Charlie C. L. Wang

***Abstract*— In this paper, we present a low-cost IMU-based system, Pedalvatar, which can capture the full-body motion of users in real-time. Unlike the prior approaches using the hip-joint as the root of forward kinematic model, a foot-rooted kinematic model is developed in this work. A state change mechanism has also been investigated to allow dynamically switching the root of kinematic trees between the left and the right foot. Benefitted from this, full-body motions can be well captured in our system as long as there is at least one static foot in the movement. The 'floating' artifact of hip-joint rooted methods has been eliminated in our approach, and more complicated motions such as climbing stairs can be successfully captured in real-time. Comparing to those vision-based systems, this IMU-based system provides more flexibility on capturing outdoor motions that are important for many robotic applications.**

I. INTRODUCTION

The full-body motion capture technology has a variety of applications in robotics, entertainment, virtual reality, rehabilitation and athletic training [1]–[9]. The major techniques of full-body motion capture can be classified into a few categories, including optical with active markers, optical markerless (also called image-based methods), inertial, magnetic, mechanical and acoustic tracking systems. A survey of body motion capture technology in robotics can be found in [10].

Optical motion capture systems like Vicon [11] use active markers attached on the user's body to capture the motion in a specific indoor environment. This kind of system can accurately record both the posture and the position of users when the markers are visible to the camera system. However, as the setup of camera system is not portable, the applications are limited to indoor scenarios. Image-based approaches obtain motion data directly from video streams using computer stereo vision techniques [12]. Although it is markerless, the reconstruction of body motion is less accurate than the active marker based methods. Due to the huge amount of data to be processed, it is hard to capture full-body motion in real-time. Recently, the depth-image based technique [9] has become popular in the entertainment applications, with the help of which real-time motion capture and reconstruction can be realized on a consumer-level PC. Nevertheless, this approach suffers from the same drawbacks of all vision-based motion capture systems. When part of the human body is hidden by obstacles, the motion can only be predicted so that will have large errors. On the other aspect, there is requirement on the distance between the depth camera and the human body. Moreover, the success of motion capture is very sensitive to the illuminance. These factors significantly reduce the flexibility of using such technique for capturing outdoor motions.

Mechanical systems use wearable exoskeletons to directly measure the joint angles between articulated body segments instead of estimating the positions of points on the body. These systems offer good portability. One major drawback is that the weight of exoskeletons can easily make it uncomfortable to wear. Furthermore, mechanical systems usually can only measure angles in one degree-of-freedom (DOF) [13], which limits the types of motions to be captured.

Acoustic systems usually compute the locations of markers by using the time-of-flight of an acoustic signal. A number of emitters are worn by the user and a set of receivers are installed at fixed positions around the environment of motion capture. The location of each emitter is determined by its distances to different receivers. These systems usually have high accuracy in tracking but the signal interference is serious when a large number of emitters are installed. Moreover, as the locations of receivers must be fixed and determined through a calibration procedure, such systems must be integrated with other types of sensors to capture a large-ranged outdoor motion (e.g., [3]). The inertial tracking system has become more popular recently because of its portability, which provides the capability of motion capture in a large working envelope. An inertial motion capture system usually has a combination of accelerometers, gyroscopes and magnetometers (e.g., [14]), and the data obtained from different sensors is then fused by sensor fusion algorithms to obtain the orientation and the relative position. It is usually called *Inertial Measurement Unit* (IMU). Systems based on IMU do not need to install fixed cameras (or receivers) around the environment of motion capture. Therefore, it has the ability to capture the large-ranged outdoor motion with little burden.

IMU-based sensors are initially designed to track the orientation of aerial vehicles. When being used in the motion capture of human bodies, they are not good at capturing positions without the help of other devices. The *Global Position System* (GPS) and barometers are employed in prior work, where GPS provides the absolute position and a barometer can offer the absolute altitude. However, GPS can only provide large-scale measurement of motions, which are not qualified to be used in motion capture of human bodies. And the response speed of a barometer is too slow for real-time motion capture (e.g., the motion capture speed

All the authors are with the Department of Mechanical and Automation Engineering, The Chinese University of Hong Kong, Shatin, N.T., Hong Kong; Corresponding Author: Charlie C. L. Wang (E-mail: cwang@mae.cuhk.edu.hk).

of our system is 50 frames/second). Floor-Westerdijk et al. [15] use inertial sensors to estimate the displacement of the center of mass by integration of the acceleration. To correct drifting errors, the *zero-velocity-updates* (ZUPT) algorithm [16] is adopted to find the location while regular walking is practiced. It is not surprising to find that for an individual without any tool, he will never know where he is. All that can be known is how many steps he has moved forward or how many stairs he has claimed up (or down). In other words, we are measuring the earth by our feet. This observation motivates our research on developing a foot rooted kinematic model and applying it to realize an IMU-based real-time motion capture system.

Our work presented in this paper has the technical contribution in the following aspects:

- A foot rooted kinematic model to capture a variety of motions as long as there is a static foot;
- A state machine to control the switch of roots to reconstruct full-body motions;
- An IMU-based body motion capture system that can be used outdoor to capture motions in real-time.

As a result, all motions with at least one static foot can be captured and reconstructed in real-time by our system.

II. OVERVIEW OF SYSTEM

This section briefs the devices and setup in our motion capture system, Pedalvatar. We also introduce the method to align the frames of IMU sensors with the frames of a human body.

A. System device and sensor data

Our motion capture system consists of thirteen *inertial measurement units* (IMU), where each IMU module (CJMCU Nano-Ahrs) integrates a three-axis accelerometer (ADXL345), a three-axis gyroscope (ITG-3200), a three-axis magnetometer (HMC5843) and a micro controller. The communication between IMU modules and the host computer is based on bluetooth. As shown in Fig.1, these IMU modules are attached at different parts of a human body with the help of elastic belts. During the motion capture, each part of a human body is assumed to conduct a rigid motion, the orientation of which will be sensed by an IMU module. The *direct cosine matrix* (DCM) algorithm presented in [17], [18] is employed to fuse the data captured by multiple sensors in an IMU module into a rotation matrix, $\mathbf{R}_S^G$, that indicates the orientation of the sensor frame S with reference to the world coordinate system G.

B. Calibration of frames

The DCM algorithm computes the rotation matrix between a sensor frame and the world coordinate system. Each sensor is associated with a body part. If the relationship between a senors frame and its related body frame can be found, we are able to use the rotation matrix generated from an IMU module to obtain the rotation matrix of a body part. Note that, we assume an invariant relationship between the sensor frames and the body frames (i.e., $\mathbf{R}_B^S$) during the motion capture. Therefore, we go through a procedure at the very beginning to align the frames of sensors with the body frames.

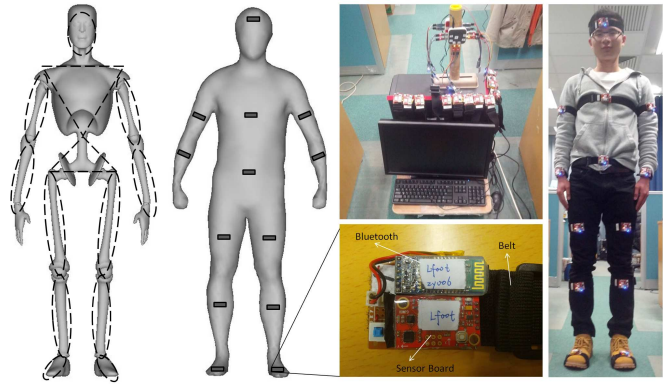

Fig. 1: Our system consists of thirteen IMU modules (as illustrated by the black bars in the middle figure) that are worn at different parts of a human body. The IMU modules communicate with the host computer via bluetooth. The sensor frames are associated with the body frames in our system via a calibration procedure with human bodies standing at N-pose [5] – see the right figure for a human body in N-pose.

There are three different frames in our system:

- G: the frame of the world coordinate system;
- S: the frame of an IMU-based sensor;
- B: the frame of a body part worn the above sensor.

Without loss of generality, the orientation of B in the world coordinate system G (i.e., $\mathbf{R}_B^G$) is pre-defined for a particular posture (e.g., N-pose introduced in [5]). The orientation of S in G (i.e., $\mathbf{R}_S^G$) can be obtained by the aforementioned DCM algorithm. Therefore, we need to calculate $\mathbf{R}_B^S$, which maps the sensor frames to the body frames as

$$\mathbf{R}_B^G = \mathbf{R}_B^S \mathbf{R}_S^G. \tag{1}$$

For a restrict rotational matrix, $\mathbf{R}_S^G$, we obtain $\mathbf{R}_B^S$ by

$$\mathbf{R}_B^S = \mathbf{R}_B^G (\mathbf{R}_S^G)^{-1} = \mathbf{R}_B^G (\mathbf{R}_S^G)^T \tag{2}$$

as $(\mathbf{R}_S^G)^{-1} = (\mathbf{R}_S^G)^T$. This calibration procedure is taken on all the IMU modules, where every one is associated with a body part with predefined body frame in N-pose. In total, thirteen $\mathbf{R}_B^S$ matrices can be obtained. They will be used in the real-time motion capture to generate the orientations of body frames according to the sensor frames by Eq.(1). The origins of body frames will be obtained by the forward kinematic model introduced below.

III. FOOT ROOTED KINEMATIC MODEL

Poses of a human body during the motion capture can be reconstructed by a forward kinematic model in the tree structure (see Fig.3 for an example). Traditional methods (e.g., [15], [19]) usually treat the center of hip as the root of a kinematic tree. They simulate the path of the hip's center in certain moving patterns to reconstruct human motions.

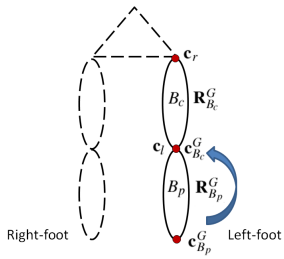

Fig. 2: An illustration for using forward kinematic model to determine the origin $\mathbf{c}_{B_c}^G$ of a child component B_c from the parent component B_p's origin, $\mathbf{c}_{B_p}^G$. When different roots (left-foot or right-foot) are employed, the origin of B_c should be located at different places (i.e., $\mathbf{c}_l$ and $\mathbf{c}_r$ respectively).

Reasonable results can be obtained in walking. However, apart from activities like walking in which the center of hip moving in a repeating and obvious pattern, it is hard to accurately describe the moving pattern of a human body at the center of hip in most general motions. Furthermore, even for walking, we cannot simulate the motions of different individuals with the same pattern. Another serious problem of the hip rooted kinematic model is the 'floating' artifact, where the reconstructed motion behaves like a marionette controlled by strings. To reconstruct a more realistic motion in real-time, we introduced the foot rooted kinematic model, in which the feet of human bodies are treated as the roots of kinematic trees.

Without loss of generality, we consider a component B_p as the parent of another component B_c on the kinematic tree. Their orientation matrices, $\mathbf{R}_{B_p}^G$ and $\mathbf{R}_{B_c}^G$, can be obtained from the IMU modules by Eq.(1). We need to determine the origin $\mathbf{c}_{B_c}^G$ of the body frame on B_c from the origin of B_p's body frame, $\mathbf{c}_{B_p}^G$. As illustrated in Fig.2, it can have

$$\mathbf{c}_{B_c}^G = \mathbf{c}_{B_p}^G + \mathbf{R}_{B_p}^G \cdot \mathbf{c}_{B_c}^{B_p} \tag{3}$$

for B_c being the child of B_p. The vector $\mathbf{c}_{B_c}^{B_p}$ is relative coordinate of $\mathbf{c}_{B_c}^G$ in the coordinate system of B_p – the value of $\mathbf{c}_{B_c}^{B_p}$ depends on the dimensions of human models. For the same component of a human body, it may have different origins when the kinematic trees with different roots are used. For example, if B_c in Fig.2 is the left thigh of a human body, the origin will be $\mathbf{c}_l$ if the root is left-foot and will be $\mathbf{c}_r$ for a right-foot rooted kinematic tree.

Rather than binding the root on a specific foot, the root of our kinematic model is dynamically switched between feet during the movement of human bodies. The state-machine for dynamic root switch will be introduced in the next section. When different roots are selected, different forward kinematic trees are used to reconstruct the poses of a human body. Fig.3 shows the trees rooted at left-foot and right-foot, where the corresponding rotation matrices on different body frames are also given. Following the order given by a forward kinematic tree, the origin of each body frame can be determined one by one. In our implementation, we convert the body frame (e.g., B) into a transformation matrix to be

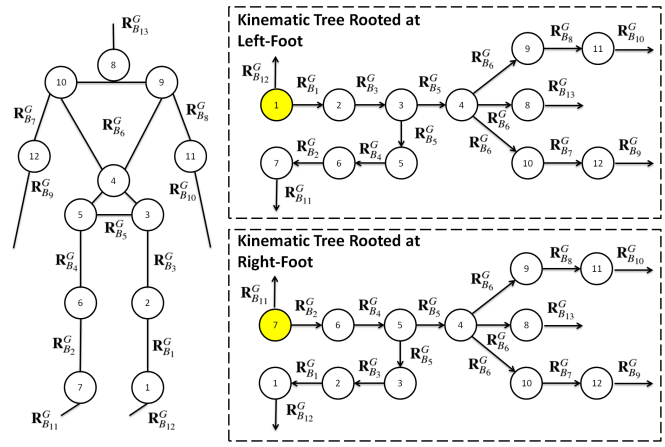

Fig. 3: The forward kinematic trees rooted at different feet where the root nodes are displayed in yellow.

applied to every points belonging to the same part as

$$\mathbf{T}_B = \begin{pmatrix} \mathbf{R}_B^{B^0} & \mathbf{c}_B^{B^0} \\ 0 & 1 \end{pmatrix}, \tag{4}$$

where

$$\mathbf{R}_B^{B^0} = \mathbf{R}_B^G (\mathbf{R}_{B^0}^G)^{-1} = \mathbf{R}_B^G (\mathbf{R}_{B^0}^G)^T \quad \text{and} \quad \mathbf{c}_B^{B^0} = \mathbf{c}_B^G - \mathbf{c}_{B^0}^G$$

with $\mathbf{R}_{B^0}^G$ and $\mathbf{c}_{B^0}^G$ being the orientation and the origin of body frame on the virtual avatar represented by a triangular mesh. Applying $\mathbf{T}_B$s to the vertices on the virtual avatar can deform it into the same pose as the user worn IMUs.

As will be explained, there are some moments that both the left-foot and the right-foot are static. Our system treats such case as both-root. The forward kinematic tree shown in Fig.4 is employed. It can find that the position of joint $\mathbf{c}_4$ can be determined both from the left-foot as

$$\mathbf{c}_4' = \mathbf{c}_{B_1}^G + \mathbf{R}_{B_1}^G \mathbf{c}_{B_1}^{B_2} + \mathbf{R}_{B_3}^G \mathbf{c}_{B_2}^{B_3} + \mathbf{R}_{B_5}^G \mathbf{c}_{B_3}^{B_4}$$

and from the right-foot as

$$\mathbf{c}_4'' = \mathbf{c}_{B_7}^G + \mathbf{R}_{B_2}^G \mathbf{c}_{B_7}^{B_6} + \mathbf{R}_{B_4}^G \mathbf{c}_{B_6}^{B_5} + \mathbf{R}_{B_5}^G \mathbf{c}_{B_5}^{B_4}.$$

Obviously, there is no guarantee that $\mathbf{c}_4' = \mathbf{c}_4''$. A simple method to solve this contradiction is to assign $\mathbf{c}_{B_4}^G = \frac{1}{2}(\mathbf{c}_4' + \mathbf{c}_4'')$. A more sophisticated solution is to slightly update the rotation matrices, $\mathbf{R}_{B_{1\ldots5}}^G$, to resolve the error on $\mathbf{c}_{B_4}^G$. Specifically, letting

$$\tilde{\mathbf{R}}_{B_{1\ldots5}}^G = \mathbf{R}_{B_{1\ldots5}}^G + \triangle \mathbf{R}_{B_{1\ldots5}}^G$$

we can then try to determine the values of $\triangle \mathbf{R}_{B_{1\ldots5}}^G$ by

$$\begin{aligned} &\mathbf{c}_{B_1}^G + \tilde{\mathbf{R}}_{B_1}^G \mathbf{c}_{B_1}^{B_2} + \tilde{\mathbf{R}}_{B_3}^G \mathbf{c}_{B_2}^{B_3} + \tilde{\mathbf{R}}_{B_5}^G \mathbf{c}_{B_3}^{B_4} \\ &= \mathbf{c}_{B_7}^G + \tilde{\mathbf{R}}_{B_2}^G \mathbf{c}_{B_7}^{B_6} + \tilde{\mathbf{R}}_{B_4}^G \mathbf{c}_{B_6}^{B_5} + \tilde{\mathbf{R}}_{B_5}^G \mathbf{c}_{B_5}^{B_4}. \end{aligned} \tag{5}$$

A least-norm solution of $\triangle \mathbf{R}_{B_{1\ldots5}}^G$ can be obtained for this under-determined problem. According to our experimental tests, the simple solution for determining $\mathbf{c}_{B_4}^G$ by averaging $\mathbf{c}_4'$ and $\mathbf{c}_4''$ gives acceptable results in most case. The rarely happened abnormal cases can be quickly resolved after a few steps as our system reconstructs the pose of a human body

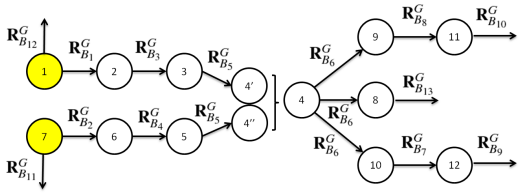

Fig. 4: The forward kinematic tree rooted at both the left-foot and the right-foot. The contradiction between $\mathbf{c}_4'$ and $\mathbf{c}_4''$ should be resolved to determine the origin of upper body.

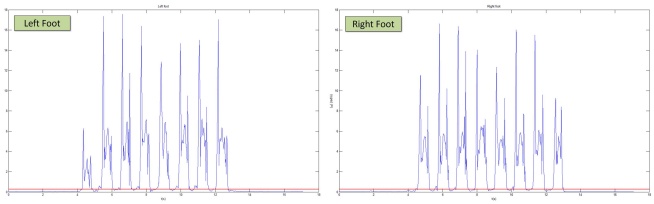

Fig. 5: Magnitudes of angular velocities measured on IMU sensors mounted on feet – the data is captured while walking slowly. The red line is the threshold τ used in our state-machine for activating the root switch.

by applying transformation on the initial pose (i.e., the errors will not be accumulated).

IV. DYNAMIC ROOT SWITCH

From the kinematic model introduced above, it is easy to know that the detector of state-change plays a very important role in our system. During the movement of a human body, we need to dynamically switch the states of motion among the left-foot rooted mode, the right-foot rooted mode, and the both-feet rooted mode. In gait analysis, the *zero-velocity-updates* (ZUPT) technique was used in [16] to correct the drift in the integration of acceleration. We are motivated by this idea to determine the root switch of forward kinematic trees. To detect the zero velocity event on feet, the angular velocities generated by gyroscopes on the two IMU sensors mounted on feet are transferred to the host computer to drive the state machine for root switching. Fig.5 shows the signals of angular velocity (in magnitude) measured on two IMU sensors mounted on feet in the example of walking. These signals will be used to drive the change of states.

In our system, four states are presented. The event of state change is activated by checking the norm of angular velocities according to the following conditions

$$\begin{cases} 1: & \text{if } \|\omega_L\| \geq \tau \ \& \ \|\omega_R\| < \tau \\ 2: & \text{if } \|\omega_L\| < \tau \ \& \ \|\omega_R\| \geq \tau \\ 3: & \text{if } \|\omega_L\| < \tau \ \& \ \|\omega_R\| < \tau \\ 4: & \text{if } \|\omega_L\| \geq \tau \ \& \ \|\omega_R\| \geq \tau \end{cases} \tag{6}$$

where each event is mapped to a state-change shown in Fig.6. $\|\cdots\|$ gets the norm of angular velocity vector. The value of threshold, τ, used to determine whether one foot is moving can be obtained by studying the walking pattern of two feet as shown in Fig.5. When the tester walks slowly to generate a walking pattern, we can determine the value of τ

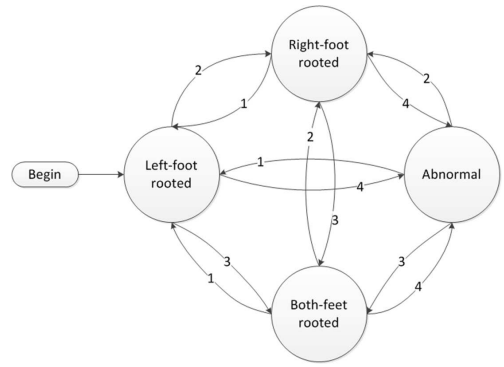

Fig. 6: State-machine used in our system for switching the roots of forward kinematic trees.

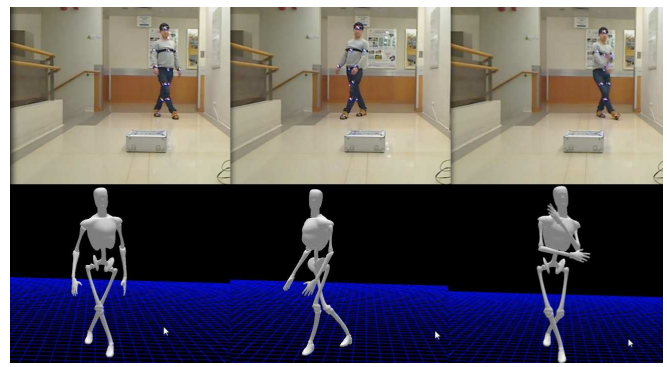

Fig. 7: Example of dancing captured by our system.

by minimizing the cases of both static (event 3 above) and the cases of both moving (event 4 above). Neither overlap nor gap happens at this level. Here, overlap means both feet are moving and gap denotes both are static, which do not match the real case of non-stop walking. $\tau = 0.28$ is obtained from our tests and employed in the demo system. Note that, when both feet's velocities are greater than τ, our system will alarm this abnormal case and keep the pose of human body unchanged.

To improve the robustness of our system, we introduce a window when monitoring the state change. Not only the velocities at the current (i.e., ω_L^i and ω_R^i) but also the velocities in previous 1 2 time currents (i.e., ω_L^{i-1}, ω_R^{i-1}, ω_L^{i-2} and ω_R^{i-2}) are employed to activate the state change. Then, the conditions of state-change presented in Eq.(7) are modified to

$$\begin{cases} 1: & \text{if } \min\{\|\omega_L^{i-k}\|\} \geq \tau \ \& \ \max\{\|\omega_R^{i-k}\|\} < \tau \\ 2: & \text{if } \max\{\|\omega_L^{i-k}\|\} < \tau \ \& \ \min\{\|\omega_R^{i-k}\|\} \geq \tau \\ 3: & \text{if } \max\{\|\omega_L^{i-k}\|\} < \tau \ \& \ \max\{\|\omega_R^{i-k}\|\} < \tau \\ 4: & \text{if } \min\{\|\omega_L^{i-k}\|\} \geq \tau \ \& \ \min\{\|\omega_R^{i-k}\|\} \geq \tau \end{cases} \tag{7}$$

with $k = 0, 1, 2$ for each condition. The state-machine runs more robustly when these conditions are used.

V. RESULTS AND VERIFICATION

We have implemented the proposed approach by using Processing [20], an open-source language and environment,

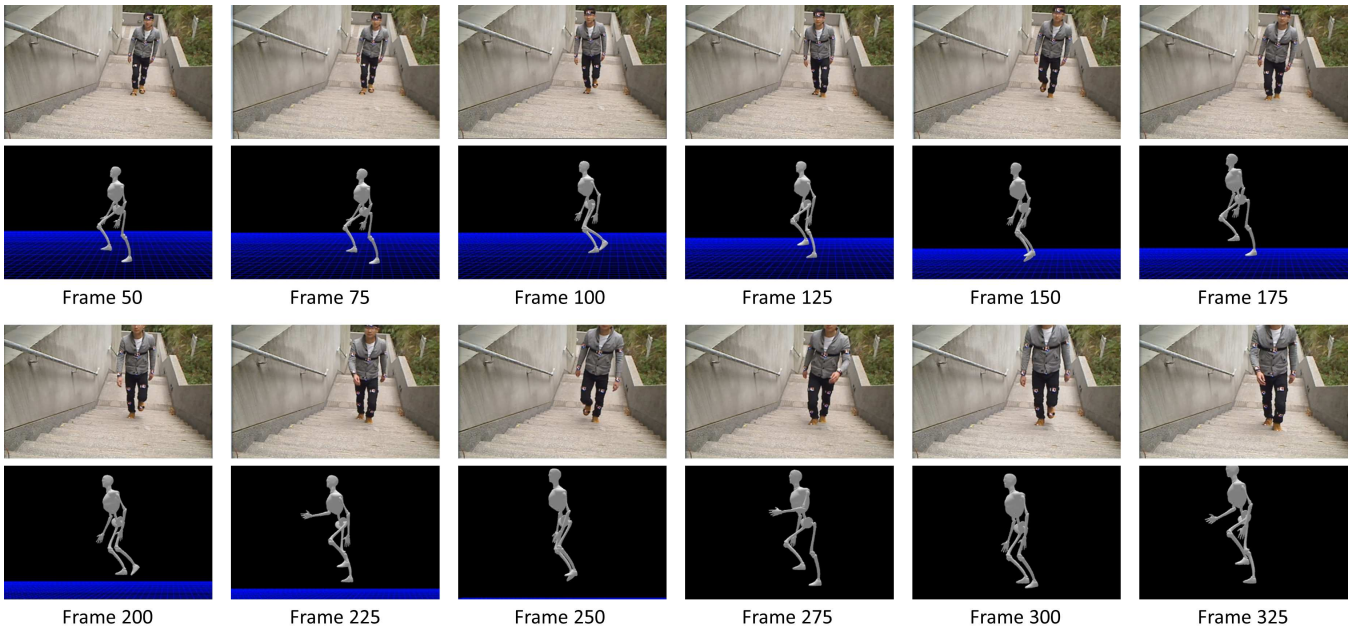

Fig. 9: Example of outdoor motion – climbing up stairs that can be successfully captured and reconstructed by our system.

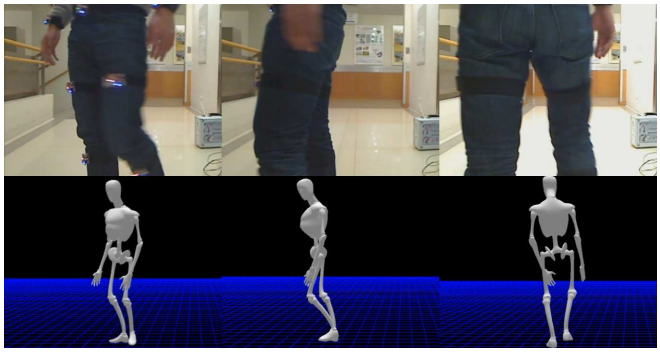

Fig. 8: Example of walking and turning around captured by our system.

running on Windows 7 OS. The IMU modules are programmed by Arduino [21]. The communication between IMU modules and the host computer is realized by bluetooth. The system can capture the full-body motions based on 13 sensors in real-time (i.e., around 50 frames/second). The tests are all taken on a PC with Intel Core i5-4570 CPU at 3.20GHz + 8GB RAM. A variety of motions have been tested by our system. It is found that many human activities can fulfill the condition of at least one foot being static – for example, dancing, Kongfu and walking (with turning around) motions shown in Figs.7-8. These motions can generate many cases with vision obstacles in vision-based systems (e.g., Vicon and Kinect), which cause challenging problems for motion capture in real-time. Our system does not suffer from vision obstacles. A more challenging outdoor motion – climbing up the stairs has also been tested. As shown in Fig.9, the motion reconstructed by our system can fully realize the position and the altitude change during the movement. A video of motions captured by our system can be accessed at: `http://youtu.be/Exsc6gODi3E/`.

The verification is taken at both the level of sensors and the level of systems. To conduct the verification of IMU sensor's performance, the rotation matrix obtained from the DCM algorithm is decomposed into Euler angles (i.e., yaw, pitch and roll). The three angles are then verified respectively. A horizontal table equipped with a compass as shown in the top row of Fig.10 is employed to provide the ground truth. The error measurements on yaw, pitch and roll are shown in the bottom row of Fig.10. It can be found that the angles in yaw contains larger errors than pitch and roll as the measurement in yaw is more sensitive to the magnetic interference in the testing environment.

For the verification taken at the system level, we measure the positions of hand and feet in the motions along specific trajectories. In the test using hand, we let the tip of hand move along the boundary of a 50cm x 50cm foam board. The result is compared with the ground truth in Fig.11. The test on feet is taken by walking along a straight line with 4.71m and then turning around to walk back to the starting point. As can be see in Fig.12, the trajectory measured by our system has been drifted with a distance around 0.4m, which is mainly caused by the interference of magnetic fields and the detection errors of foot switch. We will develop a more robust state-machine in the future research.

VI. CONCLUSION

In this paper, we presents, Pedalvatar, a low-cost IMU-based motion capture system that can capture six degrees-of-freedom full body motion in real-time as long as there is at least one static foot at each time step. A foot-rooted kinematic model and the dynamic switching algorithm has been developed to reconstruct the motion of human bodies

	Yaw	Pitch	Roll
L^2-Error	0.5681 deg.	0.1595 deg.	0.2414 deg.
L^∞-Error	4.150 deg.	1.140 deg.	1.740 deg.

Fig. 10: Verifications for the accuracy of sensors – the setups for measuring yaw (left), pitch (middle) and roll (right) are shown in the top row. The bottom table lists the errors measured on yaw, pitch and roll respectively.

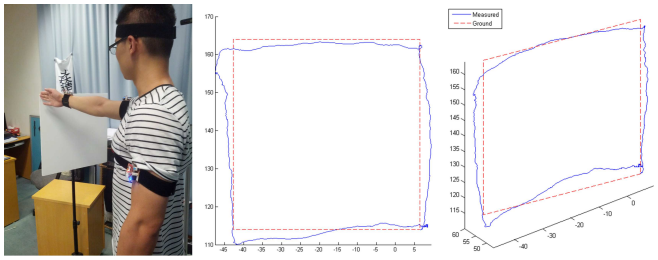

Fig. 11: The trajectory of hand's tip captured by our system is compared with the ground truth – the boundary of a board.

from the orientation data generated by the IMU sensors. Comparing to prior methods using hip-rooted kinematics, our approach does not have the 'floating' artifact in the reconstructed motions. With the observation that there are a large variety of motions fulfill the condition of static foot, this system can be used in many applications of robotics.

Our current system cannot successfully reconstruct the motion with both feet moving very fast (e.g., running and jumping). However, as the acceleration information of feet can be obtained from the IMU attached on feet, this system is able to be extended to obtain the root of kinematic tree by analyzing the speed change of feet. Our planned work in the near future is to study the integration of foot acceleration to get positions in running and jumping, and investigates the possibility of extending the ZUPT technique in these cases to enhance our state-machine.

ACKNOWLEDGMENT

Part of this research is supported by the research project CUHK/7050392, and we also would like to thank the technical support provided by Allan Mok at CUHK.

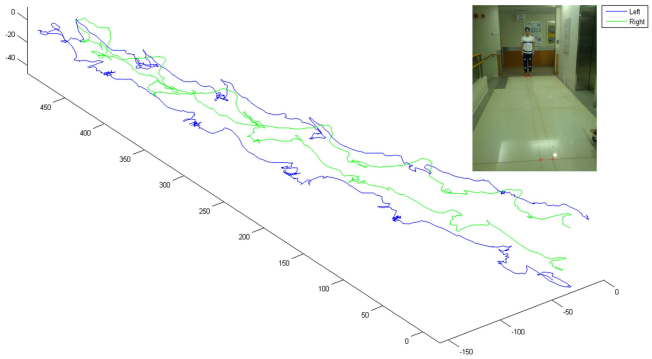

Fig. 12: The trajectory of walking forward along a straight line with 4.74m, turning around and walking back to the origin, where the accumulated location error is around 0.4m.

REFERENCES

[1] Y. Masuda, M. Sekimoto, M. Nambu, Y. Higashi, T. Fujimoto, K. Chihara, and Y. Tamura, "An unconstrained monitoring system for home rehabilitation," *IEEE Engineering in Medicine and Biology Magazine*, vol. 24, no. 4, pp. 43–47, 2005.

[2] H. Zhou, H. Hu, N. D. Harris, and J. Hammerton, "Applications of wearable inertial sensors in estimation of upper limb movements," *Biomedical Signal Proc. and Control*, vol. 1, no. 1, pp. 22–32, 2006.

[3] D. Vlasic, R. Adelsberger, G. Vannucci, J. Barnwell, M. Gross, W. Matusik, and J. Popović, "Practical motion capture in everyday surroundings," *ACM Trans. on Graphics*, vol. 26, no. 3, p. 35, 2007.

[4] T. Cloete and C. Scheffer, "Benchmarking of a full-body inertial motion capture system for clinical gait analysis," in *30th IEEE Annual International Conference of Engineering in Medicine and Biology Society*. IEEE, 2008, pp. 4579–4582.

[5] D. Roetenberg, H. Luinge, and P. Slycke, "Xsens MVN: Full 6DOF human motion tracking using miniature inertial sensors," Technical Report of Xsens Motion Technologies BV, 2009.

[6] G. F. Welch, "History: The use of the kalman filter for human motion tracking in virtual reality," *Presence: Teleoperators and Virtual Environments*, vol. 18, no. 1, pp. 72–91, 2009.

[7] Q. Yuan, I.-M. Chen, and S. P. Lee, "SLAC: 3D localization of human based on kinetic human movement capture," in *IEEE International Conference on Robotics and Automation (ICRA)*, 2011, pp. 848–853.

[8] K. D. Nguyen, I.-M. Chen, Z. Luo, S. H. Yeo, and H.-L. Duh, "A wearable sensing system for tracking and monitoring of functional arm movement," *IEEE/ASME Trans. on Mechatronics*, vol. 16, no. 2, pp. 213–220, 2011.

[9] J. Shotton, A. Fitzgibbon, M. Cook, T. Sharp, M. Finocchio, R. Moore, A. Kipman, and A. Blake, "Real-time human pose recognition in parts from single depth images," in *Proceedings of the 2011 IEEE Conference on Computer Vision and Pattern Recognition*. IEEE Computer Society, 2011, pp. 1297–1304.

[10] M. Field, Z. Pan, D. Stirling, and F. Naghdy, "Human motion capture sensors and analysis in robotics," *Industrial Robot: An International Journal*, vol. 38, no. 2, pp. 163–171, 2011.

[11] "Vicon motion capture systems," http://www.vicon.com.

[12] Y. Chen, J. Lee, R. Parent, and R. Machiraju, "Markerless monocular motion capture using image features and physical constraints," in *Computer Graphics International 2005*. IEEE, 2005, pp. 36–43.

[13] M. Zecca, F. Cavallo, M. Saito, N. Endo, Y. Mizoguchi, S. Sinigaglia, K. Itoh, H. Takanobu, G. Megali, O. Tonet, *et al.*, "Using the waseda bioinstrumentation system WB-1R to analyze Surgeon's performance during laparoscopy - towards the development of a global performance index," in *2007 IEEE/RSJ International Conference on Intelligent Robots and Systems*. IEEE, 2007, pp. 1272–1277.

[14] S. Beeby, *MEMS mechanical sensors*. Artech House, 2004.

[15] M. J. Floor-Westerdijk, H. Schepers, P. H. Veltink, E. H. van Asseldonk, and J. H. Buurke, "Use of inertial sensors for ambulatory assessment of center-of-mass displacements during walking," *IEEE Transactions on Biomedical Engineering*, vol. 59, no. 7, pp. 2080–2084, 2012.

[16] E. Foxlin, "Pedestrian tracking with shoe-mounted inertial sensors," *IEEE Comp. Graph. and App.*, vol. 25, no. 6, pp. 38–46, 2005.

[17] W. Premerlani and P. Bizard, "Direction Cosine Matrix IMU: Theory," http://gentlenav.googlecode.com/files/DCMDraft2.pdf.

[18] "DCM Tutorial An introduction to orientation kinematics," http://www.starlino.com/dcm_tutorial.html.

[19] T. Koritnik, T. Bajd, and M. Munih, "A simple kinematic model of a human body for virtual environments," in *Advances in Robot Kinematics: Motion in Man and Machine*, J. Lenarcic and M. M. Stanisic, Eds. Springer Netherlands, 2010, pp. 401–408.

[20] "Processing," http://processing.org.

[21] "Arduino," http://http://www.arduino.cc.